SCINTIGRAPHIC QUANTIFICATION OF LYMPHATIC FUNCTION: BAYESIAN INFERENCE ON DIFFUSION DYNAMICS

Petr Gebouský[1], **Miroslav Kárný**[1], **Anthony Quinn**[2]

[1]*Department of Adaptive Systems*
Institute of Information Theory and Automation
Academy of Sciences of the Czech Republic
Prague, CZECH REPUBLIC

[2]*Department of Electronic and Electrical Engineering*
University of Dublin, Trinity College
Dublin, IRELAND

E-mail: gebousky@utia.cas.cz

Abstract: Lymphoscintigraphy is a sensitive diagnostic technique in nuclear medicine. One of its principal applications is the investigation of upper limb lymphedema. Typically, only two or three snapshots of the distribution of the radioactive tracer in the limb can be obtained, so that traditional inferences of important physiological indicators are completely unreliable. In this paper, the Bayesian paradigm, exploiting available prior information in conjunction with a simplified model of the diffusion dynamics, is used to obtain new reliable quantitative evaluations applicable under routine.

Keywords: signal processing, decision making, model identification, Bayesian estimation, sparse data, upper limb lymphedema, quantitative lymphoscintigraphy

1 INTRODUCTION

The power of the Bayesian paradigm is evident in inference problems based on a few measurements only. Nuclear medicine is a rich and important application domain where problems of this type are the norm. Quantitative diagnostics for lymphedema of the upper limbs is a case in point. The contributions of the paper are: (a) quantitative lymphoscintigraphy, unavailable until now, is developed and tested; (b) standard Bayesian tools are shown to solve a surprisingly wide range of real tasks; and (c) the modeling role of the Bayesian paradigm is underlined.

Secondary lymphedema—excessive arm swelling caused by a damaged lymphatic system—is a frequently occurring side-effect of breast cancer treatment. It can be simply corrected when diagnosed correctly at a early latent stage. Late stages are hard to cure and often lead to full disability. Lymphoscintigraphy, i.e. imaging of the time-dependent dispersion of the injected radionuclide, is the used frequently to complement clinical inspections (Svensson *et al.*, 1999; Pain *et al.*, 2002). It visualizes the regional lymph drainage system in a sensitive and non-invasive way. Structural and functional information is yielded at the injection depot, along the extremity, and over regional lymph nodes. Qualitative morphologic inspection is sufficient for late disease stages. Diagnostics for the critical early stage are poorly supported, with results depending enormously on the skill of the inspecting expert. There have been efforts of scintigraphy quantification, since the partial results indicated better sensitivity in detection of latent lymphedema (Weissleder and Weissleder, 1988). However, reliable quantitative evaluation is currently missing. The main reason is that the condition of the patient, as well as economic and time factors, allow only two or three scans of the extremities. A Bayesian attack appears to be the only viable remedy.

2 LYMPHOSCINTIGRAPHIC DATA

In a standardized inspection, about 25MBq of ^{99m}Tc-labeled albumen is injected into interstitial space of both hands. The scintigraphic images of the radio-tracer visualize the accumulation and flow of the carried serum through the lymphatic system of the limb. Its time evolution reflects the state of a patient's lymphatic system.

One minute images are taken immediately after injection, then after about 30 and 180 minutes. Correction for physical decay is made and regions of interest (ROI) specified. Fig. 1 shows typical ROIs around the axillary nodes, the upper and lower halves of the arm respectively. Local 'calibrated' relative activities for each image are computed as the total count over each ROI normalized by the total count in the complete first image reflecting the administered activity.

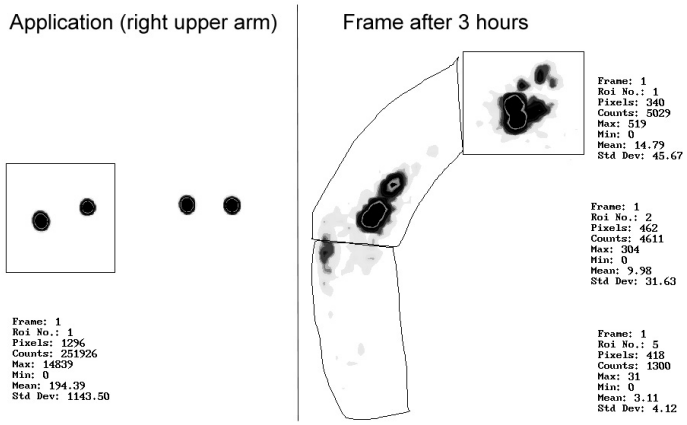

Fig. 1: Scintigraphic images of upper arm with the definition of regions.

3 A PARAMETRIC SYSTEM MODEL

Let t be the number of minutes since the administration time at $t = 0$. Hence, real time is $\tau(t) = t\Delta$, $\Delta = 1$ [min]. The actual sampling moments are $\mathcal{T} = (t_1, \ldots, t_N)$. Their number N is small. The *relative* amount of the injected tracer is a *unit impulse*, i.e. $u_t = \delta(t)$ where $\delta(0) = 1$ and $\delta(t) = 0$, for $t \neq 0$. The discrete-time scalar *impulse response* x_t of the lymphatic system at the chosen ROI, known as the *time activity curve*, is the relative integral count at time $\tau(t)$ over ROI pixels. Causality implies that $x_t = 0$ for $t < 0$.

The dynamic model relating the sequences u_t and x_t, see Fig. 2(a), is chosen as a cascade of first-order linear models, with a common parameter a for each of the d sections, and with a single lumped gain parameter, b. It is chosen as a compromise between the complex distributed nature of the lymphatic system and the need for a model with few unknown parameters. This cascading of simple sections describes the gradual penetration of serum through the limb.

Binomial expansion of the system denominator leads to the difference equation:

$$x_t = -\sum_{i=1}^{d} \binom{d}{i} (-a)^i x_{t-i} + b u_t. \tag{1}$$

For $u_t = \delta(t)$, x_t is the *impulse response* of the lymphatic system observed at times t at the particular ROI. Its closed form solution (Oppenheim *et al.*, 1999) is:

$$x_t = b \binom{t+d-1}{t} a^t, \quad t \geq 0. \tag{2}$$

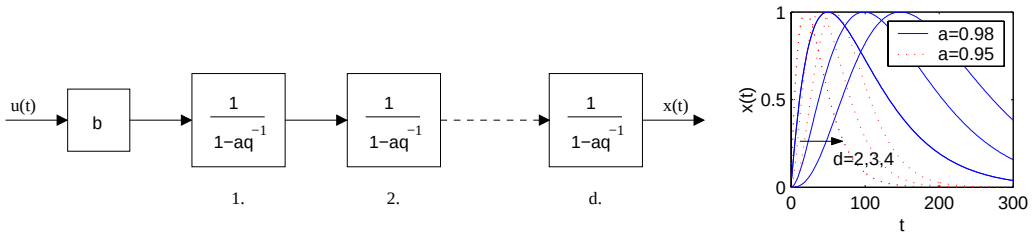

(a) Parametric cascade model. (b) Impulse response

Fig. 2: Modeling of scintigraphic time activity curves at a particular ROIs. (a) Input-output dynamic model cascading identical first-order linear sections (q^{-1} is the backward shift operator, $q^{-1}x_t = x_{t-1}$); (b) its impulse responses for various a, d (b normalized).

A rich signal ensemble is generated by the proposed parametric model. It successfully captures the stable, slowly-decaying, non-oscillatory nature of the lymphatic system responses at a particular ROI with only three free parameters. In particular, the order parameter, d, allows a rich set of candidate curves to be explored, including those exhibiting a convex nature. Typical normalized curves are illustrated in Fig. 2(b).

The time activity curve, evaluated at the observation moments $\tau(t)$, $t \in \mathcal{T}$, is gathered into the N-vector $X = (x_{t_1}, x_{t_2}, \ldots, x_{t_N})^T$ (^{T} denotes transposition). Hence:

$$X = bA_\vartheta,\ A_{\vartheta,i} = \binom{t_i + d - 1}{t_i} a^{t_i},\ i = 1, \ldots, N,\ \vartheta = (a, d)^T. \tag{3}$$

Noisy samples y_t of the time activity curves are observed. As emphasized in Section 2, measurements, y_t, are normalized, aggregated counts for the ROI at time t. Individual counts have a Poisson distribution, but aggregation permits the overall noise effect to be approximated well by additive zero-mean normal noise e_t, i.e. $y_t = x_t + e_t$. Infrequent sampling implies that measurements are approximately independent. The variance r of noise e_t can be assumed (approximately) constant. Thus, the probability density function (pdf) for the N-vector of observations $Y = (y_1, y_2, \ldots, y_{t_N})^T$, is:

$$p(Y|\mathcal{T}, \Theta) = (2\pi r)^{-0.5N} \exp\left(-\frac{1}{2r}||Y - bA_\vartheta||^2\right). \tag{4}$$

$||\cdot||$ denotes the Euclidean norm. The observation model is parameterized by the quadruple $\Theta = (a, b, d, r)$. The pdf $p(Y|\mathcal{T}, \Theta)$ depends on the set of actual observation times, via $\mathcal{T}$.

4 PRIOR INFORMATION AND BAYESIAN ESTIMATION

Parameters Θ are unknown, and require prior distributions to be elicited. The variance, r, is a property only of the measurement process.Thus, for its estimation, data from various ROIs and patients can be used. The remaining three parameters are strictly local to the ROI and the patient. They have to be estimated using two or three measurements. This is impossible without prior information, which is rich in this case. This is the key advantage of the Bayesian paradigm in the inference of diagnostically significant quantities from the sparse data. The prior information is expressed through intervals of *a priori* possible Θ, given with comments in the following list:

- $a = \vartheta_1$ $\quad (0 < a < 1)$ — the inspected responses are stable and non-oscillatory; the interval is shrunk to reflect practically observed slow accumulation dynamics (typically $a = \vartheta_1 \in (0.9, 0.999)$); specific values depend on model order.
- $d = \vartheta_2$ $\quad (1 < d \leq \overline{d} \approx 6)$ — the parameter describes the penetration rate through the limb and modifies the curve shape; the current experience indicates that 6 is the conservative upper bound of the model order.

- b $(0 < b < \overline{b}_\vartheta)$ — the response is non-negative and cannot exceed the applied input $u_0 = 1$ (the maximum $\overline{b}_\vartheta$ as a function of ϑ is evaluated numerically).
- r $(10^{-6} < r < 10^{-4})$ — the range corresponds with interval (0.5%, 25%) of the noise in the observed signal; smaller values of r are more probable due to averaging over ROIs; the variance is *a priori* independent of other parameters. This range can be gradually improved by processing of many sets of ROI data.

The mixed-type prior distribution $p(\Theta)$ can be written as a product of conditional distributions in accordance with the relationships in the above list:

$$p(\Theta) = p(a, b, d, r) = p(b|a, d, r)p(a|d)p(d)p(r) = p(b|\vartheta, r)p(a|d)p(d)p(r).$$

The variance r is included in the first factor to simplify evaluations.

The unknown continuous parameter $a = \vartheta_1$ enters the observation model in a nonlinear way (2). To get a feasible solution, it has been discretized. The polynomial dependence on a indicates that the influence of a decays exponentially. This motivates selection of a uniform grid on $\exp(a)$. The order d is naturally a discrete-valued quantity. A uniform pf on the *a priori* expected range is selected. In both cases, the uniform distribution is justified via the principle of insufficient reason (Jeffreys, 1985).

The remaining pdfs on continuous-valued b and r are expressed in conjugate form (Berger, 1985). This flexible choice simplifies evaluations. For the gain b, the Gaussian pdf is conjugate. Thus:

$$p(b|\vartheta, r) = (2\pi\omega_\vartheta r)^{-0.5} \exp\left(-\frac{1}{2\omega_\vartheta r}||b - \hat{b}_\vartheta||^2\right),$$

where $\omega_\vartheta > 0$ and $\hat{b}_\vartheta$ determine this prior. The expected range of b gives $\hat{b}_\vartheta = 0.5\overline{b}_\vartheta,\ \omega_\vartheta = \overline{b}_\vartheta^2/(4\hat{r})$, where $\hat{r}$ is a conservative estimate of the measurement variance r leading to a relatively flat constructed prior pdf. The adopted choice corresponds to one standard deviation on both sides of the mean. The conjugate prior for estimation of $r > 0$ is:

$$p(r) = \left(\frac{(\delta - 2)\varepsilon}{2}\right)^{0.5\delta} \Gamma^{-1}(0.5\delta)\, r^{-0.5\delta - 1} \exp\left(-\frac{(\delta - 2)\varepsilon}{2r}\right).$$

$\Gamma(\cdot)$ is the Euler gamma function. This pdf is parameterized by $\varepsilon > 0$ and $\delta > 0$. It has expectation ε and variance $\frac{2\varepsilon^2}{\delta - 4}$. Use of the Gaussian approximation of this pdf and the physical confidence interval, with half-width equal to one standard deviation, give the choice $\delta = 7,\ \varepsilon = 3 \times 10^{-5},\ \hat{r} = 10^{-5}$. A more resolved choice is unnecessary as the interval serves only as an initial conservative guess for specification of the prior pdf on b. It also initializes the estimation of r, which can be improved with each patient.

The Bayesian estimator (Berger, 1985; Peterka, 1981) combines the observation model $p(Y|\Theta)$ (4), the quantified prior information $p(\Theta)$ and the relative activities, Y, measured over a ROI at sampling moments $\mathcal{T}$, into the posterior pdf:

$$p(\Theta|\mathcal{T}, Y) = \frac{\omega_\vartheta^{-\frac{1}{2}} r^{-\frac{N+\delta+3}{2}} p(\vartheta)}{C p(Y|\mathcal{T})} \exp\left[-\frac{1}{2r}\left(||Y - bA_\vartheta||^2 + (\delta - 2)\varepsilon + \omega_\vartheta^{-1}||b - \hat{b}_\vartheta||^2\right)\right]. \quad (5)$$

The normalizing constant C, independent of measured values Y and measurement moments $\mathcal{T}$, is uniquely implied by the normalization of pdfs. The predictive pdf $p(Y|\mathcal{T})$ in the denominator is used for determining a good set of sampling time indices, $\mathcal{T}$. Introducing the normalized

quantities, $B_\vartheta = \sqrt{\omega_\vartheta} A_\vartheta$ and $\hat{B}_\vartheta = \hat{b}_\vartheta / \sqrt{\omega_\vartheta}$, the predictive pdf is expressed up to another normalizing constant, c, as follows:

$$p(Y|\mathcal{T}) = c \sum_{\vartheta} \frac{p(\vartheta) \left(||B_\vartheta||^2 + 1 \right)^{-\frac{1}{2}}}{\left(||Y||^2 + \varepsilon + \hat{B}_\vartheta^2 - \frac{\left(Y^{\mathrm{T}} B_\vartheta + \hat{B}_\vartheta \right)^2}{||B_\vartheta||^2 + 1} \right)^{\frac{N+\delta}{2}}}. \tag{6}$$

Note that the posterior pdf, $p(\Theta|\mathcal{T}, Y)$, is non-zero on the grid of the *a priori* allowed values of $\vartheta = (a, d)$. Correspondingly, the summation in (6) runs over these values only.

5 INFERENCE OF DIAGNOSTICALLY SIGNIFICANT QUANTITIES

The posterior pdf, $p(\Theta|\mathcal{T}, Y)$, is the start-point for computing posterior properties of unknown parameters (or functions thereof), several of which have clinical significance.

5.1 Estimation of the Expected Time-Activity Curve, $\hat{X}$

Construction of this curve has been the principal motivation for the modeling and estimation techniques described here. It follows from (1), (2) that X is a deterministic function of the unknown parameters, Θ. The distribution of the ensemble of possible X is therefore a (highly non-linear) function of the posterior pdf $p(\Theta|\mathcal{T}, Y)$. From a clinical perspective, the expected value $\mathrm{E}[X|\mathcal{T}, Y]$ is the most important characteristic of the response of the lymphatic system at some ROI, and can be calculated directly from (3), (5):

$$\hat{X} = \mathrm{E}[X|\mathcal{T}, Y] = \sum_{\vartheta} \int X(\vartheta, b) p(\vartheta, b, r|\mathcal{T}, Y) \, dbdr = \sum_{\vartheta} A_\vartheta \int b p(\vartheta, b|\mathcal{T}, Y) \, db. \tag{7}$$

The integral in (7) can be found in analytic form, and thus the numerical evaluation reduces to a simple summation over the grid of *a priori* allowed values of ϑ. The covariance matrix of X is computed similarly.

Time-activity curves for all ROIs in one limb are shown in Fig. 3. The expected value $\hat{X}$ is drawn, together with an envelope formed by intervals with widths equal to the marginal standard deviations. Similar intervals for noisy measurements Y are also included. The probability with which the time-activity curve is expected within this range can be evaluated. Even without this, the time-index of the maximum of the time-activity curve provides important qualitative information about the inspected lymphatic system.

5.2 Estimates of Model Parameters and Derived Quantities

It is expected that the parameter estimates can be used in clinical staging of lymphedema. Point or interval estimates of the elementary time constant a and the chain length d are intuitively good indicators of accumulation kinetics. They are described by the marginal posterior distribution $p(\vartheta|Y) = p(a, d|Y)$.

As well other derived quantities can be useful, e.g. residence time (e.g. Heřmanská *et al.*, 1998; Stabin, 1996) is widely accepted in nuclear medicine as a quantitative global characteristic of accumulation kinetics. With the adopted scaling, the residence time in minutes is found as the area under the time-activity curve $\xi(a, d, b) = \sum_{t=0}^{\infty} x_t \Delta$, with $\Delta = 1$[min]. This sum converges for the considered stable elementary models with $0 \leq a < 1$. Again the expected residence times and standard deviations, are the most instructive characteristics of the pdf $p(\xi|\mathcal{T}, Y)$ (see Fig. 3). Further research into clinical significance of various quantities is underway.

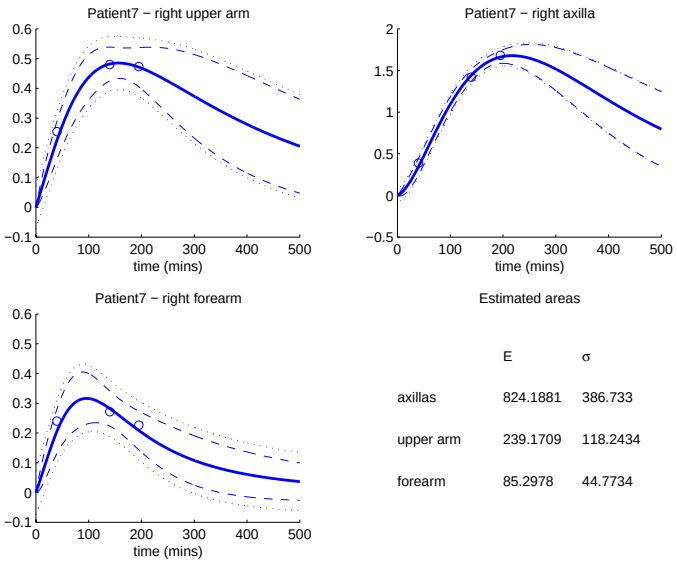

Fig. 3: Example of time-activity curves and residence times estimation. Each graph corresponds to a different ROI. The circles denote measured data. Bold solid lines represent $\hat{X}$, the time-activity curves, dashed lines their uncertainty (mean$\pm$std). Dotted lines represent uncertainty intervals for responses with noise, defined in the same way. Y-axes give % values. Estimates of the expected residence times for each ROI, and their standard deviation σ, are provided in the final quadrant of the figure.

5.3 Selection of Appropriate Sampling Times $\mathcal{S}$

This task is critical as the number of measurements is restricted in routine practice. Thus, it is desirable to advance beyond the current empirical choice of standardized sampling times. A collection of patients, measured more frequently than is the clinical norm, has provided the experimental data needed for Bayesian inference of an optimal sampling grid.

Let us consider a sub-selection $\mathcal{S} \subset \mathcal{T} = (t_1, \ldots, t_N)$ of sampling times for all patients within the considered over-sampled experimental set. Then, the predictive pdf conditioned on data with indices in $\mathcal{S}$, $p(Y|\mathcal{S}) = \int p(Y|\Theta)p(\Theta|y_t,\ t \in \mathcal{S})\, d\Theta$, can be evaluated using all data measured on the patient. By definition, the patient-specific characteristics are independent. Thus, the product of the quantities over the whole set $\mathcal{Y}$ of patient measurements provides the observation model needed for estimating the unknown optimal sub-selection $\mathcal{S}$ of sampling times. A choice of the prior distribution $p(\mathcal{S})$ (typically, uniform over available choices) and Bayes' rule provide the posterior distribution over the candidates $\mathcal{S}$, and decision theory yields the optimal choice (Gebouský and Křížová, 2000). It reduces to the *maximum a posteriori (MAP)* probability estimate of $\mathcal{S}$ if the posterior distribution $p(\mathcal{S}|\mathcal{Y})$ is peaked enough. The results presented below indicate that this simplification is tenable.

5.4 Comparison of Accumulation on Both Limbs

Comparison of the responses of a particular patient's limbs is a very useful diagnostic aid, since, often, it is known that one limb is healthy, and it can act as a control for evaluation of the other limb. It implies the need for a quantitative comparison of a small set of scintigraphic images, a task which is hopeless without a Bayesian treatment. The problem is formalized as a test of the hypothesis, H_0, that the accumulation characteristics on both limbs are the same: i.e. that they can be described by a single common model. The alternative, H_1, is defined as the need to model both limbs independently. The Bayesian decision is $\hat{H} = \arg\min_{H \in \{H_0, H_1\}} \sum_j Z(\{D_1, D_2\}, H, H_j) p(H_j|D_1, D_2)$. The loss function, Z, depends generally on the data, D_1 and D_2, for the respective limbs. $Z \geq 0$ is a $(2, 2)$ table, typically with zero diagonal entries. Positive entries reflect medical and economic consequences of a bad selection.

ROI	Time intervals [min]			
	$\mathcal{I}_1 = \langle 30, 50\rangle$	$\mathcal{I}_2 = \langle 55, 95\rangle$	$\mathcal{I}_3 = \langle 115, 150\rangle$	$\mathcal{I}_4 = \langle 175, 220\rangle$
Forearm	•		•	
Upper arm		•		•
Axilla		•		•

Table 1: Optimization results of a pair of measurement moments for ROIs (• denote optima).

Bayes' rule and the formulation of the hypotheses imply $p(H|D_1, D_2) \propto p(D_1, D_2|H)p(H)$ where:

$$\begin{aligned} H_0 : p(D_1, D_2|H_0) &= \int_\Theta p(D_1|\Theta)p(D_2|\Theta)p(\Theta)d\Theta \\ H_1 : p(D_1, D_2|H_1) &= \int_{\Theta_1} p(D_1|\Theta_1)p(\Theta_1)d\Theta_1 \int_{\Theta_2} p(D_2|\Theta_2)p(\Theta_2)d\Theta_2. \end{aligned}$$

Then, $\hat{H} = H_0$—i.e. the hypothesis of limb equality is accepted—if:

$$p(H_0|D_1, D_2) \geq \mathcal{P} = \frac{Z(\{D_1, D_2\}, H_0, H_1)}{Z(\{D_1, D_2\}, H_0, H_1) + Z(\{D_1, D_2\}, H_1, H_0)}. \tag{8}$$

6 EXPERIMENTAL RESULTS AND CONCLUSIONS

The methodology described above has been experimentally evaluated in all respects. It has been confirmed, for instance, that the pair of measurement times preferred in routine clinical practice (Section 2) has the highest posterior support among the possibilities available from the over-sampled grid (Section 5.3). The choice of the pair of sampling moments on the model quality is significant (Gebouský and Křížová, 2000). Optimization of the sampling moment pair is therefore essential.

The measurement times differ from patient to patient in the experimental set. Hence, they were grouped into sets of similar values, and measurement intervals rather than individual measurement moments were assessed. The available intervals, together with optimization results over 22 patients, are summarized in Table 1. The choice was straightforward since the posterior distribution, $p(\mathcal{S}|\mathcal{Y})$, was strongly peaked. Table 1 shows that the delayed data are important for the upper arm and axilla. This corresponds to their increasing distance from the injection site. A compromise in the choice of time intervals has to be made if it is not clear which regions are important for staging the disease. The combination $\{\mathcal{I}_2, \mathcal{I}_4\}$ seems to be the best in this respect.

Meanwhile, the estimates of time activity curves have been welcomed by physicians as a useful semi-quantitative aid for judging hand-staging.

Good results have been achieved in quantitative comparison of the upper limb pairs. Table 2, giving results for $\mathcal{P} = .95$ in (8), illustrates them on the screening tests (Barret and Swidell, 1981) for forearms of 14 patients. Limb equality was judged by a nuclear medicine expert via visual evaluation of the raw (non-reduced) scintigraphic images (ViD decisions). Clinician, who was treating the patients, made an independent judgement (CD decisions). Medical decisions serve for practical evaluation of the quantitative test (8) (QD decisions). Comparing correspondence of QD and ViD with CD, the proposed test alone gives better results then ViD (sensitivity 100% vs. 66%, specificity 80% both). These results are taken as preliminary, since the amount of available patient data is limited, and definite clinical conclusions are incomplete.

(a) CD vs. QD

Clinical	Quantitative test (QD)	
difference (CD)	T^+	T^-
C^+	9	0
C^-	1	4

(b) CD vs. ViD

Clinical	Visual sc. test (ViD)	
difference (CD)	S^+	S^-
C^+	6	1
C^-	3	4

Table 2: Comparison of clinical decision (CD) with via the proposed the proposed Bayesian test(QD) and visual (Vid) decision on forearm equality. C^+/C^- denotes the cases when the limbs are taken as the same/different from the clinical (CD) viewpoint. S^+, S^- and T^+, T^- denote corresponding values for SD and QD respectively. The number of cases belonging to the individual groups are quoted in the table.

Taking into account the discrepancies between experts, as well as the fact that non-committal prior information was used in the proposed Bayesian hypothesis test, the high degree of correspondence with the conclusions of both physicians is impressive. It underlines the enormous benefit of the Bayesian approach in lymphoscintigraphy.

ACKNOWLEDGEMENT

This research has been supported by CZ-SLO grant KONTAKT 2001/020 and partially by GA ČR 102/99/1564, AV ČR S1075102 and Project MIAPS 6458-3 from Internal Grant Agency of Ministry of Health of the Czech Republic. I want to thank doctors of the Department of Nuclear Medicine FNM for the cooperation. First of all, I wish to express my sincere gratitude to Mrs. M.D. Hana Křížová for her patient and invaluable support.

REFERENCES

Barret, H. and Swidell, W. (1981), *Radiological Imaging. The Theory of Image Formation, Detection, and Processing*, Vol. 2, Academic Press.

Berger, B. (1985), *Statistical Decision Theory and Bayesian Analysis*, Springer-Verlag, New York.

Gebouský, P. and Křížová, H. (2000), Contribution of Bayesian identification to evalution of upper limb lymphedema, Technical Report 1991, ÚTIA AV ČR, Praha.

Heřmanská, J., Kárný, M., Jirsa, L. and Němec, J. (1998), Evaluation of biophysical quantities related to the treatment of thyroid diseases, *in* 'Quantitative Image Analysis in Functional Scintigraphic Imaging', GAMAMED, Prague, pp. 39–42.

Jeffreys, H. (1985), *Theory of Probability*, Clarendon Press, Oxford.

Oppenheim, A., Schafer, R. and Buck, J. (1999), *Discrete-Time Signal Processing*, Prentice Hall.

Pain, S., Nicholas, R., Barber, R., Ballinger, J., Purushotham, A., Mortimer, P. and Peters, A. (2002), 'Quantification of lymphatic function for investigation of lymphedema: Depot clearance and rate of appeareance of soluble macromolecules in blood', *The Journal of Nuclear Medicine* **43**(3), 318–324.

Peterka, V. (1981), Bayesian system identification, *in* P. Eykhoff, ed., 'Trends and Progress in System Identification', Pergamon Press, Oxford, pp. 239–304.

Stabin, M. (1996), 'Mirdose 3 software for internal dose assesment in nuclear medicine', *Journal of Nuclear Medicine* **37**, 538–546.

Svensson, W., Glass, D., Bradley, D. and Peters, A. (1999), 'Measurement of lymphatic function with technecium-99-m-labelled polyclonal immunoglobulin', *European Journal of Nuclear Medicine* **26**(5), 504–510.

Weissleder, H. and Weissleder, M. (1988), 'Lymphedema: Evaluation of qualitative and quantitative lymphoscintigraphy in 238 patients', *Radiology* **167**(3), 729–735.